A wide-field suprachoroidal retinal prosthesis is stable and well tolerated following chronic implantation

Joel Villalobos[1,6,7], David A.X. Nayagam[1,4]*, Penelope J. Allen[2,3], Penelope McKelvie[4], Chi D. Luu[2,3], Lauren N. Ayton[2,3,9], Alexia L. Freemantle[1], Michelle McPhedran[1], Meri Basa[4], Ceara C. McGowan[1], Robert K. Shepherd[1,5], Chris E. Williams[1,4,5,8]

[1] Bionics Institute, East Melbourne VIC 3002, Australia

[2] Centre for Eye Research Australia, University of Melbourne, VIC 3002, Australia

[3] Royal Victorian Eye & Ear Hospital, East Melbourne, VIC 3002, Australia

[4] Department of Anatomical Pathology, St Vincent's Hospital, Fitzroy, VIC 2065, Australia

[5] Medical Bionics Department, University of Melbourne, VIC 3002, Australia

[6] Department of Electrical and Electronic Engineering, University of Melbourne, VIC 3010, Australia

[7] National ICT Australia, Victoria Research Laboratory, Parkville, VIC 3010, Australia

[8] Department of Surgery, University of Melbourne, VIC 3050, Australia

[9] Department of Ophthalmology, University of Melbourne, VIC 3010, Australia

Corresponding Author:

Assoc. Prof. Chris E. Williams
Bionics Institute
384-388 Albert St
East Melbourne, VIC 3002, AUSTRALIA
Tel. +61 3 9288 3523, Fax +61 3 9288 2998
Email: cwilliams@bionicsinstitute.org

* J. Villalobos and D.A.X. Nayagam contributed equally

Word count: 4712

Abstract

Purpose: The safety of chronic implantation of a retinal prosthesis in the suprachoroidal space has not been established. This study aimed to determine the safety of a wide-field suprachoroidal electrode array following chronic implantation using histopathological techniques and electroretinography.

Methods: A platinum electrode array in a wide silicone substrate was implanted unilaterally in the suprachoroidal space in adult cats (n = 7). The lead and connector were tunneled out of the orbit and positioned subcutaneously. Post-surgical recovery was assessed using fundus photography and electroretinography (ERG). Following 3 months of passive implantation, the animals were terminated and the eyes assessed for the pathological response to implantation.

Results: The implant was mechanically stable in the suprachoroidal space during the course of the study. The implanted eye showed a transient increase in ERG response amplitude at 2 weeks which returned to normal by 3 months. Pigmentary changes were observed at the distal end of the implant, near the optic disc. Histopathological assessment revealed a largely intact retina and a thin fibrous capsule around the suprachoroidal implant cavity. The foreign body response was minimal with sporadic presence of macrophages and no active inflammation. All implanted eyes were negative for bacterial or fungal infections. A mid-grade granuloma and thick fibrous build-up surrounded the extraocular cable. Scleral closure was maintained in 6 of 7 eyes. There were no staphylomas or choroidal incarceration.

Conclusions: A wide-field retinal prosthesis was stable and well tolerated during long-term suprachoroidal implantation in a cat model. The surgical approach was reproducible and overall safe.

Introduction

Degenerative retinal diseases are the leading cause of untreatable blindness. One of such diseases, retinitis pigmentosa (RP), has an estimated global prevalence of 1 in 3500[1]. Over the course of the disease process, the majority of the photoreceptors are lost, most commonly starting from the peripheral retina. Some ganglion and inner retinal cells survive, particularly in the center of the visual field[2]. Photoreceptor replacement by means of gene therapy and retinal transplantation has been clinically tested with moderate success in some disease conditions[3, 4], but is not a clinical possibility yet and is not suitable for all retinal degenerative diseases. Electrical stimulation of the visual pathway with a prosthetic device is a more promising alternative[5-7].

An initial goal for a visual prosthetic device is to improve patient mobility and supplement the use of a guide dog or a long cane. Studies have shown that orientation and mobility are well correlated with the size of visual field and contrast sensitivity in RP[8], with nearly 70% of the variance in walking speed being accounted for by these two measures[9]. A retinal prosthesis providing a wide visual field (e.g. larger than 20˚) could be effective at improving mobility[10], while achieving high resolution would potentially allow reading and face recognition[11]. There are several viable targets in the visual pathway for a prosthetic device; stimulation of the visual cortex[12, 13] or the optic nerve[14, 15] are potential alternatives, but stimulation at the retinal level provides simpler surgical access, a simple retinotopic map of the visual field and utilizes more of the existing neuronal processing. This prosthesis would need to cover a considerable area of the retina to produce wide field perception.

Several anatomical locations for electrical stimulation of the neural retina are being investigated, including epiretinal, subretinal and suprachoroidal sites. Epiretinal implants have shown promise during clinical trials in long[16, 17] and short term implantation[18-20] as well as acute testing[21, 22].

Implanted patients have shown significant improvement in detecting and counting objects and form discrimination tasks[16]. Epiretinal implantation can be safe[23] but carries the risks of surgical trauma, poor implant fixation[24], retinal reorganization due to uneven pressure from the implant[25] and retinal detachment[26]. Subretinal implants have been well tolerated in clinical trials[27] and some implanted patients have been able to recognize objects and read letters[28]. Subretinal implantation can provide stable mechanical fixation but has greater degree of surgical difficulty and there is a limit to the size of the implant and prospective visual field[29]. The risks associated with subretinal implantation include loss of the residual photoreceptor layer[30-33], reorganization of the inner retina[33], disruption of the retinal pigment epithelium[34] and surgical trauma including retinal perforations[35]. Intrascleral electrodes have been successful in eliciting percepts in blind patients in semi-chronic[36] and acute testing[37]. Suprachoroidal and intrascleral implantation for transchoroidal stimulation are safer and less demanding surgical approaches but carry the risk of bleeding[38] and retinal damage at pressure points related to implant design[39, 40]. These transchoroidal stimulation sites come at the cost of higher thresholds compared with optimally placed epi- or subretinal electrode arrays[41]. However, spatially selective excitation of the neuroretina has been shown using suprachoroidal electrodes and stimulation levels well within the safe limits for platinum electrodes[42].

A suprachoroidal retinal prosthesis is a promising alternative for a large visual field electrode array. Suprachoroidal implants have been shown to be well tolerated by the eye[43] with minimal risk of damage to the neural retina[41, 44]. The implantable electrode array needs to be designed for ease of surgical implantation, have spherical conformability[45] and robust scleral closure[40]. In this study, a wide, conformable electrode array designed for the suprachoroidal space, with a transscleral lead, was evaluated for its long-term safety following chronic implantation in normally sighted cats.

Materials and Methods

The procedures for this study were approved by the Animal Research Ethics Committee of the Royal Victorian Eye & Ear Hospital. These procedures complied with the "Australian code of practice for the care and use of animals for scientific purposes" (7th edition 2004), the "Principles of laboratory animal care" (NIH publication No. 85-23, revised 1985) and the ARVO standards for use of animals in ophthalmic research. Seven normally sighted adult cats weighing 3.7–5.5 kg were used for this study, in which the left eye was implanted with a suprachoroidal electrode array. The cat model was used because of the similarities in eye size with humans, where the cat's anteroposterior globe length is 21 mm approximately[46]. Electrical stimulation was performed in the last 2 days during an electrophysiologic experiment but the results are outside the scope of this paper. The unoperated right eye was collected as control tissue. This study evaluated the tissue response, following three months of passive implantation, using histopathological techniques.

Suprachoroidal electrode array

An array of 21 platinum (Pt) electrodes (⌀ 600 µm, 99.95% Pt; Goodfellow, Cambridge, England) was fabricated in a 19 mm × 8 mm silicone substrate as shown in Figure 1. There were also 2 Pt return electrodes (⌀ 2 mm). The substrate was tapered radially from 1 mm to a thickness of 150 µm near the edges and then slanted to a minimum thickness; this was done to improve spherical conformability and facilitate insertion[47]. The substrate was made of medical grade silicone sheet (Dow Corning, Midland, MI, USA) plus medical grade silicone adhesive (MED-1137; Nusil, Carpinteria, CA, USA), materials widely used for medical devices[48]. A silicone elastomer patch reinforced with polyethylene mesh was attached to the transscleral cable and was used to cover its exit through the sclera. A similar patch was used to attach the cable lead to the orbital margin. The Pt-Ir (90-10%) wires (Medwire; Sigmund Cohn, Mount

Vernon, NY, USA) in the cable lead terminated in an implantable connector made of Pt, reinforced silicone sheet (Bioplexus, Ventura, CA, USA) and silicone adhesive.

The electrode arrays were cleaned in detergent solution (Pyroneg; Johnson Diversey, Australia) and then rinsed in consecutive baths of ethanol, isopropanol, ethanol and distilled water. Each of these baths lasted for 5 minutes and was performed in an ultrasonic cleaner. The implants were finally autoclaved at 121°C for 30 minutes. The implants were rinsed intraoperatively in sterile normal saline for 5 minutes before implantation.

Preparation and surgery

Animals were anesthetized with an initial dose of xylazine (1 mg/kg, s.c.; Xylazil; Troy Labs, Australia) and ketamine (10 mg/kg, i.m.; Ketamil; Troy Labs)[49], and then maintained with a continuous flow of isoflurane (Delvet, Australia) in oxygen through an endotracheal tube for the remainder of the procedure.

The basic implantation procedure, which was developed in a previous study[40], was refined and adapted to ensure strong scleral closure for chronic implantation. The surgical steps used are summarized in Figure 2. First, a lateral canthotomy was performed, followed by a temporal 180˚ conjunctival peritomy. Bipolar diathermy was applied to the sclera at the temporal quadrant. A 9 mm long, full-thickness scleral incision was performed 5 mm posterior and parallel to the limbus. This was measured with Castroviejo calipers. A pocket about 5 mm deep was opened between the sclera and choroid using an angled crescent knife. The implant was tunneled under the conjunctiva and Tenon's tissue starting from the lateral orbital margin. The electrode array was then inserted into the suprachoroidal pocket and advanced 17 mm posteriorly within the suprachoroidal space. The proximal edge of the implant was inserted anteriorly under the sclera. A contact fundus lens (Quadraspheric; Volk Optical, Mentor, OH, USA) was used to check the position of the electrode array and it was advanced or retracted as necessary. The

scleral wound was closed with 8-0 nylon sutures (Ethicon; Johnson & Johnson, Australia) and the reinforced silicone patch sutured on top of the transscleral cable exit. The cable lead was looped posteriorly within the episcleral space. The cable lead was then sutured onto the zygomatic process allowing sufficient length to permit full eye movement. Range of movement was verified with a forced duction test. The cable loop was routed under the conjunctiva directly to the zygomatic process because the cat globe fills most of the orbital cavity[50]. An implantable connector at the end of the cable was inserted subcutaneously, superorostral to the pinna. The skin was closed in two layers using Vicryl stay (Johnson & Johnson) and nylon sutures.

Immediately postoperatively the eye was visually assessed for hemorrhage, retinal detachment and electrode array location, using an indirect ophthalmoscope. This assessment was repeated daily for 7 days, then at 2 weeks and then again at 3 months.

Postoperative care

After surgery, the cats were administered buprenophrine (0.01 mg/kg, s.c; Temgesic; Reckitt Benckiser, Australia) for analgesia when the anesthetic was withdrawn. For the first week the animal was given amoxicillin-clavulanate suspension once daily (10mg/kg, s.c; Clavulox; Pfizer, Italy). Topical drugs were administered twice daily for the first 14 days and tapered off as required, these included prednisolone (Prednefrin Forte; Allergan, Australia), atropine (Atropt; Sigma Pharmaceuticals, Australia) and chloramphenicol (Chlorsig; Sigma Pharmaceuticals). The drops were given until edema had resolved. All animals were checked daily for general health. Two weeks after surgery, the animals were anesthetized with ketamine-xylazine (1 and 10 mg/kg respectively, s.c.) and sutures were removed. The animals were monitored during 3 months for general health and the implanted eye was assessed visually for surgical recovery or signs of irritation.

Electroretinography assessment

An ERG was performed at 2 weeks and 3 months after implantation. Pupils were dilated with tropicamide 1% (Mydriacyl; Alcon Laboratories, Australia). The ERG was recorded using corneal contact lens electrodes (ERG-Jet; Fabrinal SA, Switzerland) on both eyes simultaneously. Flash stimuli were delivered by a Ganzfeld stimulator (ColorDome; Diagnosys LLC, Lowell, MA). An electrophysiology system (Espion E2; Diagnosys LLC) was used for stimulus generation and data acquisition. After a dark-adaptation period of 20 minutes, the ERG was recorded over a range of flash intensities (-4.0 to 1.0 log cd/m^2 in 0.3 log unit increments).

Termination and histological methods

After three months of implantation, the animals were anesthetized for an electrophysiologic experiment lasting two days. The electrodes were stimulated within an arbitrary charge density limit of 180 µC/cm^2; within the safe limits for hydrogen evolution in Pt for wide pulses[51]. The electrophysiologic findings are outside the scope of this article. The animals were then terminated with an overdose of anesthetic (150 mg/kg of sodium pentobarbital, i.v.; Pentobarbitone; Troy Labs, Australia). Heparinised saline at 37°C was perfused via the left ventricle until venous outflow was clear, followed by perfusion with 0.8–1.2 L of neutral buffered formalin (NBF) (10% solution) at 4 °C. After enucleation, the globes were cleared of the extraocular soft tissue attachments and muscle, except for the tissue surrounding the cable lead and patches. The whole globes were then post-fixed in Davidson's modified fixative for 18–24 h at room temperature, transferred into 50% ethanol for 6–8 h and stored in 70% ethanol at 4 °C until dissection[52, 53].

Following a macroscopic pathology assessment for anterior chamber hyphema or fibrosis, lens or vitreous opacity and noticeable retinal damage; the eyes were prepared for histological processing. The extraocular tissue surrounding the lead was first separated from the eye. The

electrode array was then removed from the eye by dissecting on the original scleral wound site and carefully extracting the device. The sclera was dyed with markings at 4 mm spacing from the optic nerve following the horizontal meridian (Figure 3A). The eyes were dissected and three or more narrow (2 mm) strips were cut from the implanted region at strategic locations (Figure 3B,C). The strips were taken from the following sites: 1) transversal horizontal section including implant tip region, optic disc and nasal region; 2) sagittal strip through a cross section of the implant tract, 8 mm from the optic nerve; 3) temporal transversal section including the anterior implanted region and original insertion site; 4) section from the extraocular proliferative tissue surrounding the episcleral patch; 5) section from the extraocular tissue surrounding the cable lead. In some cases, where the electrode was positioned obliquely, an additional section (parallel to section 1) was collected to include the implant tip region. Tissue strips were embedded in agar to reduce delamination artifacts[54]. Samples, supported by foam inserts, were transferred into 10% NBF for 1–3 h before processing in a standard automated cycle. Sections were stained with hematoxylin and eosin (H&E) using a standard automated process. Other special stains were processed manually using standard histological procedures.

Histopathological assessment

The stained histological slides were inspected to find one slide per site and per eye with consistent staining and completeness of section. The selected slide was assessed based on the following criteria: implant location, retinal damage, active inflammatory response, chronic inflammatory response, fibrosis, hemorrhage and other pathological changes. Degrees of retinal damage, fibrosis and inflammatory reaction were scored on a 4 level scale (*none, mild, moderate* and *severe*). Hemorrhage and retinal detachment were quantified as *present* or *absent*.

Statistical analyses

The unoperated right eyes were used as controls. The ERG response amplitudes of the implanted vs. control eyes were analyzed with a paired t-test. Categorical histopathology data was summarized in tables. Pathological 4-level scores were presented with the median or the 95% confidence interval (CI) for the median obtained from a 1-sample sign test; comparisons were performed with the non-parametric Mood's median test. Statistical analyses were performed with Minitab 16 (Minitab Inc.; State College, PA, USA) using double-tailed, 5% significance level.

Results

Postoperative observations

In all seven cases, the implant was reliably positioned in the suprachoroidal space without breaching the retina, similar to the results from acute implantation studies using a thin film electrode array[40]. The summary of surgical complications in Table 1 shows that there were no major postoperative complications such as hyphema, vitreous hemorrhage or retinal detachment. Fundus examination showed that an initial elevation of the retina over the implanted region, likely associated with edema, resolved within 2 weeks. This is consistent with previous studies of suprachoroidal implantation[55]. At 3 months postoperative, the implant tract could only be distinguished as a contrast change against the bright tapetum on color fundus photographs (Figure 4). There were no cases of staphyloma or choroidal incarceration.

A small subretinal hematoma developed in all eyes within 2 weeks postoperatively. These regions were typically 1–2 optic disc diameters in size. They were visible as a dark pigmentary changes contrasting with the reflective tapetum tissue as shown with a star in Figure 4. Only in 3 eyes were these visible intraoperatively. The hematomas developed within the first 2–3 days and then stabilized. One animal developed overt subretinal hemorrhage. This was observed as an extended elevation of the retina over the superior quadrant. The edema resolved before 7 weeks and the retina reattached leaving thin strips of pigmentary changes in the tissue.

The implants were mechanically stable during 3 months of implantation. Figure 5 shows the location of the implant outline at three different time points. Implants 03, 05 and 06 suffered an initial displacement of about 1–3 optic disc diameters within the first two weeks. The movement appeared to be rotational around the fixation point at the transscleral exit. The implants then remained stable through to the completion of the experiment.

Electroretinography

The ERG b-wave amplitude of the implanted and control eyes at 2 weeks and 3 months post-implantation are shown in Figure 6. There was a significant increase in the b-wave amplitude of the combined rod-cone bright flash ERG (1.0 log cd/m^2) in the implanted eyes compared to the control eyes at 2 weeks post-implantation (paired t-test, $P < 0.01$). This enhancement of the ERG response was temporary and returned to the normal amplitude level at 3 months post-implantation.

Histopathology

Analysis of the different tissue sampling sites showed more pronounced tissue reaction in the extraocular sections (4, 5 in Figure 3C) when compared to the intraocular sections (1, 2, 3 in Figure 3B). The median score for each pathological category, as shown in Figure 7, was different for the internal tissue sections taken from the eye and the tissue sections taken from the orbital lead region (Mood's median test $P < 0.001$ for active, chronic inflammation and fibrosis). Analyses were separated into the intraocular implant tract region and the extraocular lead region as described below.

Intraocular pathologies

The pathological scoring, as presented in Table 2, showed that intraocular pathologies had low incidence or low severity (95% CI for the median of *none* to *mild*). The typical response in all eyes was a thin layer of tissue consisting of fibroblasts and occasional macrophages or foreign body giant cells. The tissue response on the surface of the implant was 1 or 2 cells thick as shown in Figure 8G. On the scleral side of the implant the tissue response was more varied, with scattered foci of chronic inflammatory cells. A mild to moderate fibrotic layer was observed around the implant in 5 of 7 cases. At the edges of the array the inflammation was more pronounced than on the flat surfaces of the implant (Figure 8F,I), but not significantly more

active. The implant edges were well tolerated and did not create scleral deformations nor retinal detachment.

In the eye which developed subretinal hemorrhage after implantation (animal 04), there was a moderate reaction with a thicker fibrous layer, mild ongoing active inflammation and localized foci of outer retinal disruption with proliferation of retinal pigment epithelial (RPE) cells. These spots of retinal disruption were less than 300 µm wide (one is shown in Figure 9A) and they were scattered across the superior retina, where hemorrhage was observed during *in vivo* assessments. The retina was normal otherwise. In all seven cases, the retina adjacent to the electrode array appeared normal.

A mild active inflammatory reaction (scattered neutrophils) was found near the scleral incision in 6 of 7 eyes. This was accompanied by an increased chronic inflammatory response. Figure 8C shows an example of histiocytic reaction (*moderate*) in this region. The inflammatory reaction was significantly higher near the scleral incision than in the rest of the implant cavity (Mood's median test $P < 0.01$ for active and chronic inflammation, excluding animal 04 due to overt hemorrhage).

Pigmentary changes were observed macroscopically near the distal tip of the implant, as shown in Figure 4. Histological examination of these areas revealed disorganization in the choroidal melanin: pigment particles had been disrupted by the inflammatory reaction and absorbed by macrophages. An example is shown in Figure 9C. In 2 of 7 eyes there was also associated localized retinal damage. In animal 03 there was a 1.5 mm region of retinal degeneration (Figure 9B) near the implant tip and in animal 05 the retinal disruption was 200 µm wide.

In animal 07, the anterior edge of the implant body extruded through the sclera but remained under the conjunctiva. The anterior scleral tissue became contiguous with the foreign body response at the choroidal side of the implant tract, as shown in Figure 9D. Conjunctival

epithelial down-growth was found extending into the implant tract as can be seen in Figure 9E. Examination of the implants post-explantation revealed that the leads had different angles at rest with respect to the implant body plane. The lead in the implant that extruded rested at an angle of 27˚ whereas in the rest of the implants the angle was in the range of 0–13˚.

Extraocular pathologies

The response to the lead in the extraocular orbital region was more significant. A thick layer of fibrotic tissue developed around the lead and the fixation patches. This tissue was sectioned and processed as described above. Histological examination of the episcleral patch region (4 in Figure 3C) revealed that, typically, there was a dense fibrosis and granulation tissue. There were moderate numbers of neutrophils.

The reaction surrounding the lead region (5 in Figure 3C) consisted of a thicker fibrotic layer and granulation tissue plugs. Figure 10 shows an example of the tissue encapsulation around the lead with thick fibrotic tissue as a result of movement.

Discussion

A wide electrode array was well tolerated when chronically implanted in the suprachoroidal space of the eye. The surgical approach for suprachoroidal implantation, paired with a soft, tapered and conformable electrode array substrate shows promise as the basis for a viable neural prosthesis[56]. The *in vivo* observations showing a low incidence of postoperative complications were confirmed by the histopathological assessment showing mild tissue reaction. Comparison with the unoperated fellow eye[57] showed no significant changes nor disruption of the retinal function in the normally sighted cats.

The electrode array was mechanically stable in the suprachoroidal space and caused minimal tissue response. The initial recovery period was characterized by subretinal edema which typically resolved within 2 weeks. The foreign body reaction surrounding the implant tract was mild, suggesting the implant shape and materials were well tolerated by the eye. The thin histiocytic and fibrotic response is typical with silicone elastomer implants[58]. The variability of the inflammatory response found in the intraocular implant tract is not a major concern for the viability of the neural prosthesis[59]. The thin edges of the electrode array, which have been a site of concern in retinal prostheses[60], did not show a significantly greater tissue response and were well tolerated.

The retina was generally intact and functional over the implanted region. Amplitudes of the ERG showed normal retinal function after 3 months of implantation in all cats, when compared with their fellow control eye. There was increased ERG amplitude in the implanted eyes at 2 weeks postoperative. The increase in ERG amplitude after suprachoroidal implantation has been reported previously[41] and was not found to be associated with retinal damage, whereas in that same study subretinal implantation decreased the ERG amplitude in association with photoreceptor loss. Multi-focal ERG could be used in future studies to investigate the localized

functional changes at the implantation site. From the histology, focal disruptions of the outer retinal structure were only found near the inferonasal corner of the electrode array (the one closest to the optic nerve), except for animal 04 which suffered extended suprachoroidal hemorrhage and had distributed disruption foci across the retina. These distributed foci of retinal disruption, consisted of proliferation of RPE cells or photoreceptor “rosette” formation, which have been reported previously with subretinal implantation[33, 34]. This retinal dysplasia could be associated with a temporary elevation of the retina. Overall, the retina of this animal was well preserved and showed no loss of function.

The region of hyperpigmentation and occasional outer retinal disruption, near the inferonasal corner of the electrode array, was similar to the retinal disruption found in a previous study which was caused by the implant being close to the optic disc[40]. That previous publication indicated that a thin film electrode array should not be implanted closer than 2.6 mm to the optic disc in cats; it would be expected that the retinal disruption observed in the present study could be avoided by increasing the clearance from the optic disc. The retinal disruption was consistently located near the insertion point of the short posterior ciliary arteries and posterior ciliary veins in the cat[50]. The pigment disruption region could have resulted from a minor disturbance of the ciliary vessels with the implant edge. This would explain the slow evolution of the pigmented region over the course of 2–3 days and one case of extensive suprachoroidal hemorrhage. It is known that bleeding behind the RPE appears dark and round with fundoscopic examination[61]. Localized hyperpigmentation in cat and dog retinas has been reported in retinal prosthesis studies with epiretinal, subretinal, suprachoroidal and intrascleral implantation[30, 33, 39, 62-64]. In those studies, hyperpigmentation was associated with focal tissue disruption and it did not compromise the integrity of the inner retina for electrical stimulation. These issues could be investigated further *in vivo* using optical coherence tomography, which was not available during this study.

In comparison to this suprachoroidal approach, epiretinal and subretinal implantation appear to carry a risk of mechanical damage to the retina due to direct contact with the implant. Even though clinical trials with epiretinal and subretinal implants have been successful, the risks of trauma to the retina make the implantation of a wide-field electrode array difficult via those approaches. Subretinal implantation is known to cause photoreceptor loss at the implanted region[30, 32, 33, 65-67], with associated retinal reorganization and activation of Müller cells[68]; conveys the risk of retinal detachment[64] or retinal perforation[35]; and is limited in the size of the implant which can be held by the retinal tissue[29]. Epiretinal implantation carries the risk of retinal damage due to surgical trauma[23]; retinal tack insertion[69]; disruption due to contact or pressure[25, 70]; plus the unsecure fixation may cause the implant to move[24] or become detached[16]. These risks appear to be related to the shape and mechanical properties of the device, in which case a wider field device would likely increase their incidence. Implanting multiple devices in an eye remains an unexplored avenue for extending the visual field.

This study features the surgical implantation of a wide-field device into a suprachoroidal cleavage plane, created by advancing the device against the inner surface of the sclera which provides mechanical support. Consequently, manipulation of the reorganized retina[71] and thinned choroid[72] in RP patients would be minimized. The wide-field implant substrate with 21 electrodes at the distal tip was tolerated in the cat suprachoroidal space. The visual field covered by the array could be extended with more electrodes to cover the full 19 mm × 8 mm area of the substrate. On the other hand, the visual acuity achievable in a clinical setting would depend not only on the number of electrodes but also on other factors including: distance to the retina, pathophysiological status of the retina, stimulation-dependent shunting of currents[42] and stimulation strategies[73, 74]. Covering a wide visual field and minimizing damage to the retina are the initial goals.

In the present study, the tissue reaction over the anterior end of the implant, at the scleral incision site, was moderate. This could have spread from the more severe extraocular tissue reaction. It is also likely that the movement from the extraocular lead during fixation saccades was transferred to the implant substrate. As a result, the mechanical stress could have caused the increased inflammation observed at this site. In the single case where the implant extruded out of the sclera, the cable lead was defective with a high angle against the implant body. Here, the force from cable fixation was likely to produce constant outward pressure from the implant body on the sclera, which is known to be relatively acellular and avascular[75] and already weakened by the application of diathermy. Slow erosion through the sclera under constant tension of an implant has been shown before[76]. The reaction caused by this anterior part of the implant would be improved by designing the lead and scleral patch to minimize mechanical forces on the implant body.

Outside the eye, there was a thick capsule of proliferative tissue surrounding the lead. The granulation tissue with ongoing active inflammation indicates the presence of continued irritation, probably due to movement. This is likely to develop into a thick fibrous capsule[58], where the ongoing irritation is contained and isolated from the rest of the tissue. The inflammatory reaction observed at 3 months was probably not fully resolved and may take longer to evolve into a mature tissue response.

The foreign body reaction associated with the large electrode array was mild, indicating it was mechanically stable and biocompatible. Mild pigmentary disruption and occasional focal damage to the outer retina occurred at the inferonasal corner of the implant substrate. The retina over the electrodes remained largely intact in all cases. It has been shown previously from animal studies that suprachoroidal implantation results in no obvious damage to the eye structures[38, 44, 55]. The main risks found were suprachoroidal bleeding by disruption of the vessels, which occurred in 1 of 7 cats, and implant extrusion through the sclera. Improved

fixation of the lead and careful surgical insertion of the implant would minimize the chance of these injuries.

In summary, a wide, spherically contoured, suprachoroidal electrode array made of Pt and silicone was safe, mechanically stable and showed promise to be used as a wide-field retinal prosthesis. The surgery was reproducible and overall safe with only minor intraocular changes observed. These preclinical results support the development of a clinical device using a thin suprachoroidal electrode array.

Acknowledgements

The authors wish to thank Mark McCombe for assistance with surgeries, Helen Feng for implant manufacturing, Sue Pierce and Elisa Borg for animal care and Rebecca Argent for assistance with imaging. This work was performed at the Bionics Institute at St. Vincent's Hospital, and the Centre for Eye Research from the University of Melbourne at the Royal Victorian Eye and Ear Hospital. Funding was provided by the Ian Potter Foundation and the Australian Research Council through its Special Research Initiative in Bionic Vision Science and Technology grant to Bionic Vision Australia (BVA). The Bionics Institute acknowledges the support it receives from the Victorian Government through its Operational Infrastructure Support Program

References

1. Hartong DT, Berson EL, Dryja TP. Retinitis pigmentosa. *Lancet* 2006;368:1795-1809.
2. Humayun MS, Prince M, de Juan E, Jr, et al. Morphometric analysis of the extramacular retina from postmortem eyes with retinitis pigmentosa. *Invest Ophthalmol Vis Sci* 1999;40:143-148.
3. Bramall AN, Wright AF, Jacobson SG, McInnes RR. The genomic, biochemical, and cellular responses of the retina in inherited photorreceptor degenerations and prospects for the treament of these disorders. *Annu Rev Neurosci* 2010;33:441-472.
4. Musarella MA, MacDonald IM. Current concepts in the treatment of retinitis pigmentosa. *Journal of Ophthalmology* 2011;2011:Article ID 753547.
5. Loewenstein JI, Montezuma SR, Rizzo JF, III. Outer retinal degeneration; an electronic retinal prosthesis as a treatment strategy. *Arch Ophthalmol* 2004;122:587-596.
6. Zrenner E. Will retinal implants restore vision? *Science* 2002;295:1022-1025.
7. Dagnelie G. Retinal implants: emergence of a multidisciplinary field. *Curr Opin Neurol* 2012;25:67-75.
8. Marron JA, Bailey IL. Visual factors and orientation-mobility performance. *Am J Optom Physiol Opt* 1982;59:413-426.
9. Geruschat DR, Turano KA, Stahl JW. Traditional measures of mobility performance and retinitis pigmentosa. *Optom Vis Sci* 1998;75:525-537.
10. Ameri H, Ratanapakorn T, Ufer S, Eckhardt H, Humayun MS, Weiland JD. Toward a wide-field retinal prosthesis. *J Neural Eng* 2009;6:035002.
11. Suaning GJ, Lovell NH, Schindhelm K, Coroneo MT. The bionic eye (electronic visual prosthesis): a review. *Aust NZ J Ophthalmol* 1998;26:195-202.
12. Brindley GS, Lewin WS. The sensations produced by electrical stimulation of the visual cortex. *J Physiol* 1968;196:479-493.
13. Torab K, Davis TS, Warren DJ, House PA, Normann RA, Greger B. Multiple factors may influence the performance of a visual prosthesis based on intracortical microstimulation: nonhuman primate behavioural experimentation. *J Neural Eng* 2011;8:035001.
14. Cai C, Li L, Li X, et al. Response properties of electrically evoked potential elicited by multi-channel penetrative optic nerve stimulation in rabbits. *Doc Ophthalmol* 2009;118:191-204.
15. Sakaguchi H, Kamei M, Fujikado T, et al. Artificial vision by direct optic nerve electrode (AV-DONE) implantation in a blind patient with retinitis pigmentosa. *J Artif Organs* 2009;12:206-209.
16. Yanai D, Weiland JD, Manjunatha M, Greenberg RJ, Fine I, Humayun MS. Visual performance using a retinal prosthesis in three subjects with retintis pigmentosa. *Am J Ophthalmol* 2007;143:820-827.
17. Humayun MS, Weiland JD, Fujii GY, et al. Visual perception in a blind subject with a chronic microelectronic retinal prosthesis. *Vision Res* 2003;43:2573-2581.
18. Klauke S, Goertz M, Rein S, et al. Stimulation with a wireless intraocular epiretinal implant elicits visual percepts in blind human. *Invest Ophthalmol Vis Sci* 2011;52:449-455.
19. Laube T, Brockmann C, Roessler G, et al. Development of surgical techniques for implantation of a wireless intraocular epiretinal retina implant in Göttingen minipigs. *Graefes Arch Clin Exp Ophthalmol* 2012;250:51-59.
20. Roessler G, Laube T, Brockmann C, et al. Implantation and explantation of a wireless epiretinal retina implant device: observations during the EPIRET3 prospective clinical trial. *Invest Ophthalmol Vis Sci* 2009;50:3003-3008.

21. Rizzo JF, III, Wyatt J, Loewenstein J, Kelly S, Shire D. Perceptual efficacy of electrical stimulation of human retina with a microelectrode array during short-term surgical trials. *Invest Ophthalmol Vis Sci* 2003;44:5362-5369.
22. Humayun MS, de Juan E, Jr, Weiland JD, et al. Pattern electrical stimulation of the human retina. *Vision Res* 1999;39:2569-2576.
23. Güven D, Weiland JD, Fujii G, et al. Long-term stimulation by active epiretinal implants in normal and RCD1 dogs. *J Neural Eng* 2005;2:S65-S73.
24. de Balthasar C, Patel S, Roy A, et al. Factors affecting perceptual thresholds in epiretinal prostheses. *Invest Ophthalmol Vis Sci* 2008;49:2303-2314.
25. Ray A, Colodetti L, Weiland JD, Hinton DR, Humayun MS, Lee EJ. Immunocytochemical analysis of retinal neurons under electrical stimulation. *Brain Res* 2009;1255:89-97.
26. Walter P, Szurman P, Vobig M, et al. Successful long-term implantation of electrically inactive epiretinal microelectrode arrays in rabbits. *Retina* 1999;19:546-552.
27. Chow AY, Chow VY, Packo KH, Pollack JS, Peyman GA, Schuchard R. The artificial silicon retina microchip for the treatment of vision loss from retinitis pigmentosa. *Arch Ophthalmol* 2004;122:460-469.
28. Zrenner E, Bartz-Schmidt KU, Benav H, et al. Subretinal electronic chips allow blind patients to read letters and combine them to words. *Proc R Soc B* 2011;278:1489-1497.
29. Sachs HG, Gabel VP. Retinal replacement - the development of microelectronic retinal prostheses - experience with subretinal implants and new aspects. *Graefes Arch Clin Exp Ophthalmol* 2004;242:717-723.
30. Chow AY, Pardue MT, Chow VY, et al. Implantation of silicon chip microphotodiode arrays into the cat subretinal space. *IEEE Trans Neural Syst Rehabil Eng* 2001;9:86-95.
31. Gekeler F, Szurman P, Grisanti S, et al. Compound subretinal prostheses with extra-ocular parts designed for human trials: successful long-term implantation in pigs. *Graefes Arch Clin Exp Ophthalmol* 2007;245:230-241.
32. Salzmann J, Linderholm OP, Guyomard JL, et al. Subretinal electrode implantation in the P23H rat for chronic stimulations. *Br J Ophthalmol* 2006;90:1183-1187.
33. Montezuma SR, Loewenstein JI, Scholz C, Rizzo JF, III. Biocompatibility of materials implanted into the subretinal space of Yucatan minipigs. *Invest Ophthalmol Vis Sci* 2006;47:3514-3522.
34. Chen J, Shah HA, Herbert C, Loewenstein JI, J F Rizzo I. Extraction of a chronically implanted, microfabricated, subretinal electrode array. *Ophthalmic Res* 2009;42:128-137.
35. Gekeler F, Kobuch K, Schwahn HN, Stett A, Shinoda K, Zrenner E. Subretinal electrical stimulation of the rabbit retina with acutely implanted electrode arrays. *Graefes Arch Clin Exp Ophthalmol* 2004;242:587-596.
36. Fujikado T, Kamei M, Sakaguchi H, et al. Testing of semichronically implanted retinal prosthesis by suprachoroidal-transretinal stimulation in patients with retinitis pigmentosa. *Invest Ophthalmol Vis Sci* 2011;52:4726-4733.
37. Fujikado T, Morimoto T, Kanda H, et al. Evaluation of phosphenes elicited by extraocular stimulation in normals and by suprachoroidal-transretinal stimulation in patients with retinitis pigmentosa. *Graefes Arch Clin Exp Ophthalmol* 2007;245:1411-1419.
38. Sakaguchi H, Fujikado T, Fang X, et al. Transretinal electrical stimulation with a suprachoroidal multichannel electrode in rabbit eyes. *Jpn J Ophthalmol* 2004;48:256-261.
39. Morimoto T, Kamei M, Nishida K, et al. Chronic implantation of newly developed suprachoroidal-transretinal stimulation prosthesis in dogs. *Invest Ophthalmol Vis Sci* 2011;52:6785-6792.
40. Villalobos J, Allen PJ, McCombe MF, et al. Development of a surgical approach for a wide-view suprachoroidal retinal prosthesis: evaluation of implantation trauma. *Graefes Arch Clin Exp Ophthalmol* 2012;250:399-407.

41. Yamauchi Y, Franco LM, Jackson DJ, et al. Comparison of electrically evoked cortical potential thresholds generated with subretinal or suprachoroidal placement of a microelectrode array in the rabbit. *J Neural Eng* 2005;2:S48-56.
42. Cicione R, Shivdasani MN, Fallon JB, et al. Visual cortex responses to suprachoroidal electrical stimulation of the retina: effects of electrode return configuration. *J Neural Eng* 2012;9:036009.
43. Zhou JA, Woo SJ, Park SI, et al. A suprachoroidal electrical retinal stimulator design for long-term animal experiments and *in vivo* assessment of its feasibility and biocompatibility in rabbits. *J Biomed Biotechnol* 2008;2008:Article ID 547428.
44. Lee SW, Seo JM, Ha S, Kim ET, Chung H, Kim SJ. Development of microelectrode arrays for artificial retinal implants using liquid crystal polymers. *Invest Ophthalmol Vis Sci* 2009;50:5859-5866.
45. Stieglitz T. Development of a micromachined epiretinal vision prosthesis. *J Neural Eng* 2009;6:065005.
46. Bertschinger DR, Beknazar E, Simonutti M, et al. A review of *in vivo* animal studies in retinal prosthesis research. *Graefes Arch Clin Exp Ophthalmol* 2008;246:1505-1517.
47. Shepherd RK, Clark GM, Pyman BC, Webb RL. Banded intracochlear electrode array: evaluation of insertion trauma in human temporal bones. *Ann Otol Rhinol Laryngol* 1985;94:55-59.
48. Curtis J, Colas A. Medical applications of silicones. In: Ratner BD, Hofman AS, Schoen FJ, Lemans JE (eds), *Biomaterials science: an introduction to materials in medicine.* San Diego, CA: Elsevier; 2004.
49. Fallon JB, Irvine DRF, Shepherd RK. Cochlear implant use following neonatal deafness influences the cochleotopic organization of the primary auditory cortex in cats. *J Comp Neurol* 2009;512:101-114.
50. Prince JH. *Anatomy and histology of the eye and orbit in domestic animals*: C. C. Thomas; 1960.
51. Brummer SB, Turner MJ. Electrical stimulation with Pt electrodes: II-Estimation of maximum surface redox (theoretical non-gassing) limits. *IEEE T Bio-Med Eng* 1977;24:440-443.
52. Agrawal RN, He S, Spee C, Cui JZ, Ryan SJ, Hinton DR. *In vivo* models of proliferative vitreoretinopathy. *Nat Protoc* 2007;2:67-77.
53. Latendresse JR, Warbittion AR, Jonassen H, Creasy DM. Fixation of testes and eyes using a modified Davidson's fluid: comparison with Bouin's fluid and conventional Davidson's fluid. *Toxicol Pathol* 2002;30:524-533.
54. Banker AS, Gonzalez C, Wiley CA, Bergeron-Lynn G, Freeman WR. The agar sandwich technique for retinal biopsy processing. *Retina* 1996;16:530-534.
55. Kim ET, Kim C, Lee SW, Seo JM, Chung H, Kim SJ. Feasibility of microelectrode array (MEA) based on silicone-polyimide hybrid for retina prosthesis. *Invest Ophthalmol Vis Sci* 2009;50:4337-4341.
56. Seligman P. Prototype to product - developing a commercially viable neural prosthesis. *J Neural Eng* 2009;6:065006.
57. Dagnelie G. Psychophysical evaluation for visual prosthesis. *Annu Rev Biomed Eng* 2008;10:339-368.
58. Vistnes LM, Ksander GA, Kosek J. Study of encapsulation of silicone rubber implants in animals, a foreign-body reaction. *Plast Reconstr Surg* 1978;62:580-588.
59. Shepherd RK, Franz BKHG, Clark GM. The biocompatibility and safety of cochlear prostheses. In: Clark G, Tong YC, Patrick JF (eds), *Cochlear Prostheses.* Ney York: Churchill Livingstone; 1990.
60. Greenberg RJ, Mann AE, Little JS, et al. Implantable retinal electrode array configuration for minimal retinal damage and method of reducing retinal stress. United States; 2008.
61. Klintworth GK. The Eye. In: Rubin E, Gorstein F (eds), *Rubin's pathology: clinicopathologic foundations of medicine*: Lippincott Williams & Wilkins; 2005.
62. Pardue MT, Ball SL, Phillips MJ, et al. Status of the feline retina 5 years after subretinal implantation. *J Rehab Res Dev* 2006;43:723-732.

63. Majji AB, Humayun MS, Weiland JD, Suzuki S, D'Anna SA, de Juan E, Jr. Long-term histological and electrophysiological results of an inactive epiretinal electrode array implantation in dogs. *Invest Ophthalmol Vis Sci* 1999;40:2073-2081.
64. Völker M, Shinoda K, Sachs H, et al. *In vivo* assessment of subretinally implante microphotodiode arrays in cats by optical coherence tomography and fluroscein angiography. *Graefes Arch Clin Exp Ophthalmol* 2004;242:792-799.
65. Gekeler F, Kobuch K, Blatsios G, Zrenner E, Shinoda K. Repeated transchoroidal implantation and explantation of compound subretinal prostheses: an exploratory study in rabbits. *Jpn J Ophthalmol* 2010;54:467-475.
66. Hämmerle H, Kobuch K, Kohler K, Nisch W, Sachs H, Stelzle M. Biostability of micro-photodiode arrays for subretinal implantation. *Biomaterials* 2002;23:797-804.
67. Yu W, Wang X, Zhao C, Yang Z, Dai R, Dong F. Biocompatibility of subretinal parylene-based Ti/Pt microelectrode array in rabbit for further artificial vision studies. *J Ocul Biol Dis Inform* 2009;2:33-36.
68. Pardue MT, Stubbs EB, Jr, Perlman JI, Narfström K, Chow AY, Peachey NS. Immunohistochemical studies of the retina following long-term implantation with subretinal microphotodiode arrays. *Exp Eye Res* 2001;73:333-343.
69. Roessler G, Laube T, Brockmann C, et al. Angiographic findings folowing tack fixation of a wireless epiretinal retina implant device in blind RP patients. *Graefes Arch Clin Exp Ophthalmol* 2011;249:1281-1286.
70. Colodetti L, Weiland JD, Colodetti S, et al. Pathology of damaging electrical stimulation in the retina. *Exp Eye Res* 2007;85:23-33.
71. Santos A, Humayun MS, de Juan E, Jr, et al. Preservation of the inner retina in retinitis pigmentosa. *Arch Ophthalmol* 1997;115:511-515.
72. Ayton LN, Guymer RH, Luu CD. Choroidal thickness profiles in retinitis pigmentosa. *Clin Exp Ophthalmol* 2012;Epub ahead of print.
73. Freeman DK, Eddington DK, Rizzo JF, III, Fried SI. Selective activation of neuronal targets with sinusoidal electric stimulation. *J Neurophysiol* 2010;104:2778-2791.
74. Dommel NB, Wong YT, Lehmann T, Dodds CW, Lovell NH, Suaning GJ. A CMOS retinal neurostimulator capable of focussed, simultaneous stimulation. *J Neural Eng* 2009;6:035006.
75. Bron AJ, Tripathi RC, Tripathi BJ. *Wolff's anatomy of the eye and orbit*. London: Arnold; 2001.
76. Gerding H. A new approach towards a minimal invasive retina implant. *J Neural Eng* 2007;4:S30-S37.

Tables

Table 1. Summary of experimental animals and postoperative complications observed.

Animal	Complications
01	None
02	None
03	Strong pigmented region superotemporal to optic disc, 3 disc diameters in size
04	Developed extended subretinal hemorrhage on superior quadrant 3 days postoperative, resolved within 7 weeks
05	None
06	None
07	None

Table 2. Histopathology assessment of the implanted cat eyes following 3 months of implantation. For each category, *implant* column summarizes the scores for sites 1 and 2 from Figure 3B, while *incision* column represents site 3.

Cat No.	Retinal damage		Active inflammation		Chronic inflammation		Fibrosis		Hemorrhage		Retinal detachment
	implant	incision	implant	incision	implant	incision	implant	incision	implant	incision	implant
01	N	N	N	Mild	Mild	Mod.	N	N	N	N	N
02	N	N	N	N	Mild	N	Mild	Mild	N	N	N
03	Mild	N	N	Mild	Mild	Mild	N	N	N	N	N
04	Mild	Mild	Mod.	Mild	Mod.	Mild	Mod.	Mod.	Present	Present	N
05	Mild	N	Mild	Mod.	Mild	Mod.	Mild	N	Present	Present	N
06	N	N	Mild	Mild	Mild	Severe	Mod.	Mild	N	N	N
07	N	N	N	Mild	Mild	Severe	Mild	Mild	N	N	N
Incidence	3	1	3	6	7	6	5	4	2	2	0

(n=7)									
Median 95% CI	None to Mild	None	None to Mild	Mild	Mild	Mild to Severe	None to Mild	None to Mild	None

Mod. = Moderate

N = None

Figure Legends

Figure 1. Suprachoroidal electrode array built in a 19 mm × 8 mm silicone substrate using platinum electrodes (21 × ⌀ 600 µm and 2 × ⌀ 2 mm). Reinforced silicone was used for the fixation patches at the episcleral (ES) and orbital margin (OM) locations.

Figure 2. Diagram of steps in surgical implantation procedure. A: canthotomy and conjunctival peritomy, B: bipolar diathermy, C: sclerotomy and suprachoroidal pocket, D: electrode array tunneling, E: implant insertion, F: scleral wound closure. Adapted from J Villalobos et al., 2012[40].

Figure 3. Diagram of histological sampling technique. A: posterior view of the eye showing the implant location in relation to the optic nerve (ON) and dye markings at 4 mm increments from the nerve. B: coronal view of eye fundus showing the suprachoroidal location of the implant with a dotted line. Thick lines indicate where tissue samples were obtained at the implant tip (1), sagittal implant cross section (2) and insertion site (3). C: temporal view showing lead and the implant body with a dotted line. Samples were obtained from the extraocular tissue proliferation over the episcleral patch (4) and over the lead (5).

Figure 4. Eye fundus image of cat 01 following 3 months of implantation with suprachoroidal electrode array. Implant outline observed as contrast change beneath retina (arrow). Pigmentary changes were observed near implant tip (star). White areas are lens reflection artifacts.

Figure 5. Implant outline position with respect to optic nerve and retinal vessels, manually digitized from fundus images. Animals 03, 05 and 06 exhibited a rotational movement of the implant from the intraoperative position (blue dotted line) to the 2 week assessment position (purple dashed line), followed by stability until the 3 month assessment (green solid line). Animals 01, 02 and 07 exhibit an overall stable position of the implant with a possible rotational

movement of less than 1 optic disc diameter. Animal's 04 implant position was not clear due to retinal elevation. Animals' 06 and 07 implants were not visible at the 3 month assessment.

Figure 6. Mean amplitude of ERG b-wave of implanted and control eyes at 2 weeks and 3 months postoperative. There was a significant increase in the b-wave amplitude of the implanted eye at 2 weeks, which returned to normal levels within 3 months. Bars represent mean and whiskers are standard deviation.

Figure 7. Median score for the pathologies observed in 7 implanted eyes, including fibrosis, active and chronic Inflammation, grouped by tissue sampling site. Sections 1 to 3 are intraocular and 4 to 5 are extraocular as shown in Figure 3B,C. Extraocular pathologies were pronounced in comparison to intraocular (Mood's median $P < 0.001$).

Figure 8. Representative histological images following 3 months of suprachoroidal implantation in cat eyes. H&E stain. A: scleral incision site corresponding to site 3 in Figure 3B. Squares indicate higher magnification panels. B: implant tract detail with intact temporal retina and mild foreign body reaction. Arrows indicate location and trajectory of implant. C: detail of incision site near transscleral lead exit with moderate inflammation (triangle). D: implant tract cross-section, corresponding to tissue site 2 in Figure 3B. E: intact retina and choroid over implant tract with mild foreign body reaction (star), implant trajectory is perpendicular to image plane. F: implant lateral edge location with intact retina and mild foreign body reaction (star). G: detail of foreign body response 1-2 cells thick on implant surface adjacent the choroid. H: distal end of the implant with optic nerve and nasal retina, corresponding to site 1 in Figure 3B. I: implant distal edge location with mild fibrosis (circle). Bar = 1 mm for panels A, D and H; bar = 100 µm for panels B, C, E, F, G and I.

Figure 9. Histological images of atypical pathologies in implanted cat eyes. H&E stain. A: foci of retinal reorganization with RPE proliferation (star), found scattered in animal 04. B: focus of localized retinal degeneration (star) found at the implant tip in animal 03, where pigment

disruption occurred in choroidal tissue. C: detail of choroidal pigment disruption, melanin particles are gathered inside macrophages. D: incision site of animal 07 where the implant extruded through the sclera (triangle). E: detail of pars plana tissue beneath implant extrusion site where conjunctival downgrowth (circle) was found intruding into the implant tract. Bar = 100 µm for panels A, B, C and E; bar = 1 mm for panel D.

Figure 10. Representative histological images of the extraocular tissue response around the lead. H&E stain. A: typical fibrotic/inflammatory response around the moving extraocular cable. B: detail of thick fibrotic tissue. C: detail of granular tissue with ongoing active inflammation and hemorrhage. Bar = 500 µm for panel A; bar = 50 µm for panels B and C.

Figures

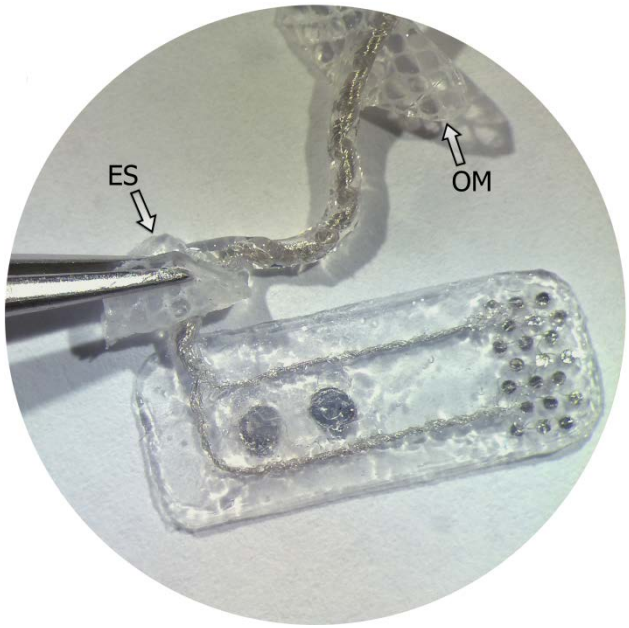

Fig. 1

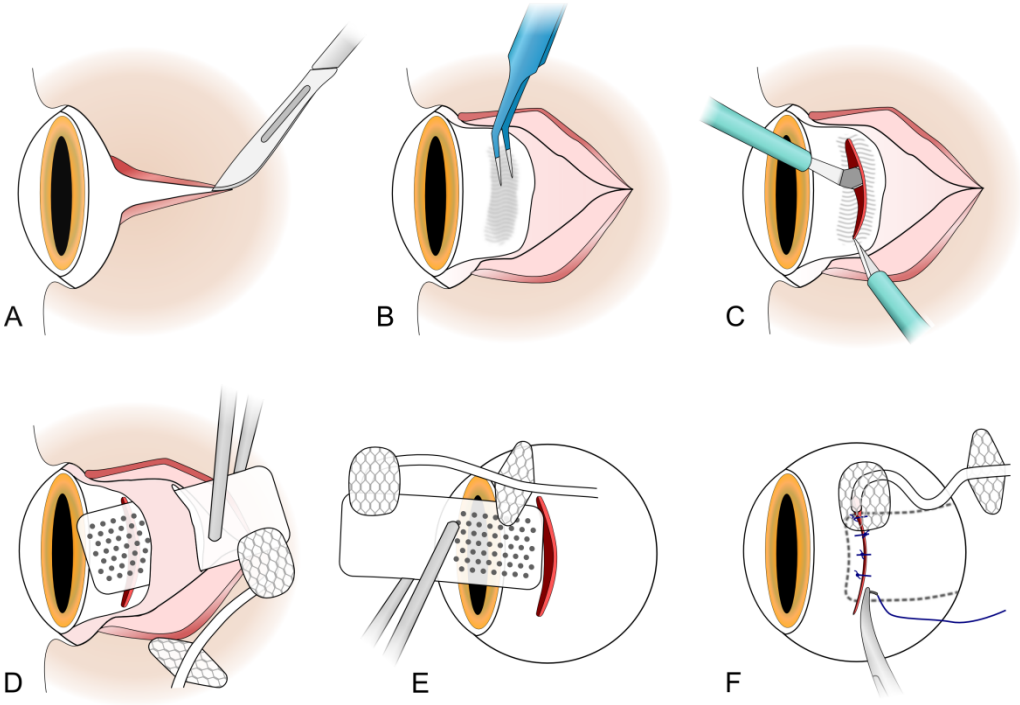

Fig. 2

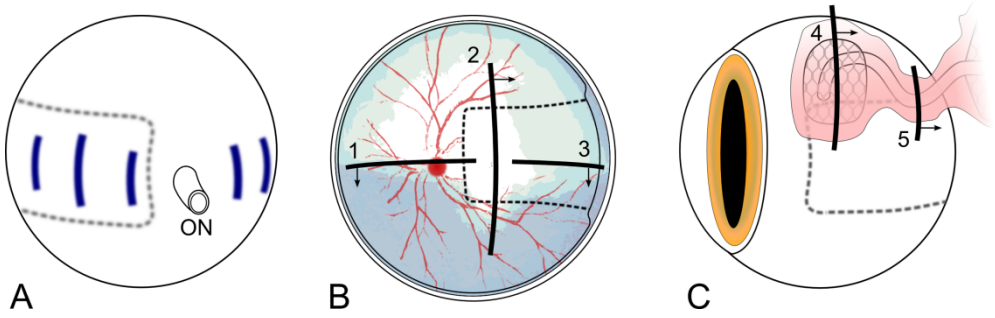

Fig. 3

Fig. 4

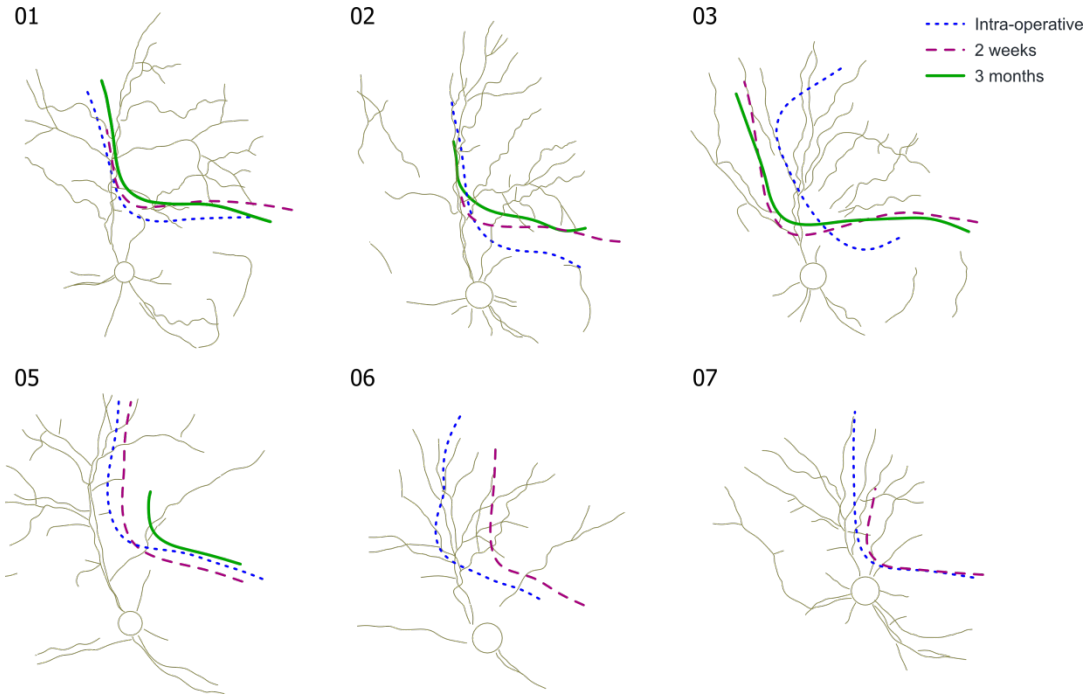
01
02
03
Intra-operative
2 weeks
3 months
05
06
07

Fig. 5

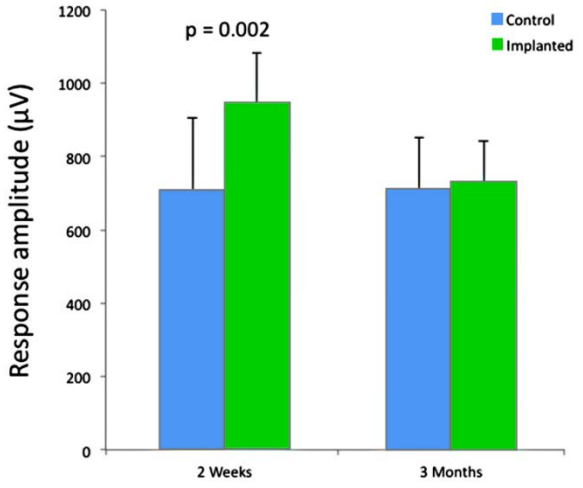
p = 0.002
Control
Implanted
Response amplitude (µV)
1200
1000
800
600
400
200
0
2 Weeks
3 Months

Fig. 6

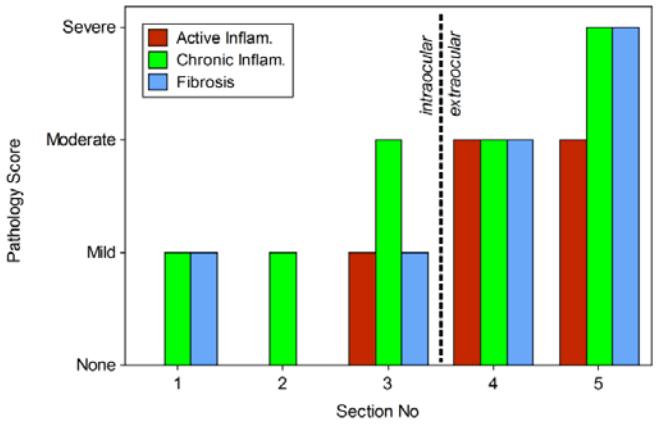
Severe
Moderate
Mild
None
Pathology Score
Active Inflam.
Chronic Inflam.
Fibrosis
intraocular
extraocular
1
2
3
4
5
Section No

Fig. 7

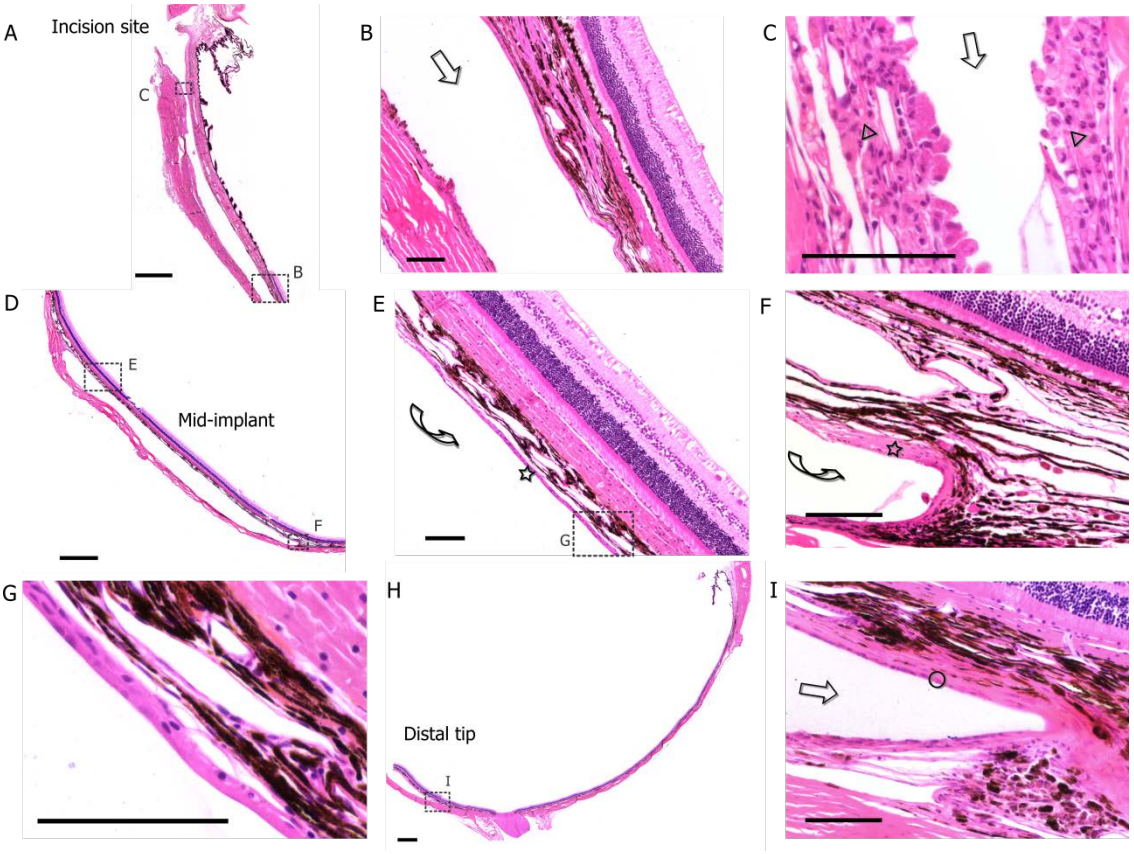
A
Incision site
B
C
D
E
Mid-implant
F
G
H
Distal tip
I

Fig. 8

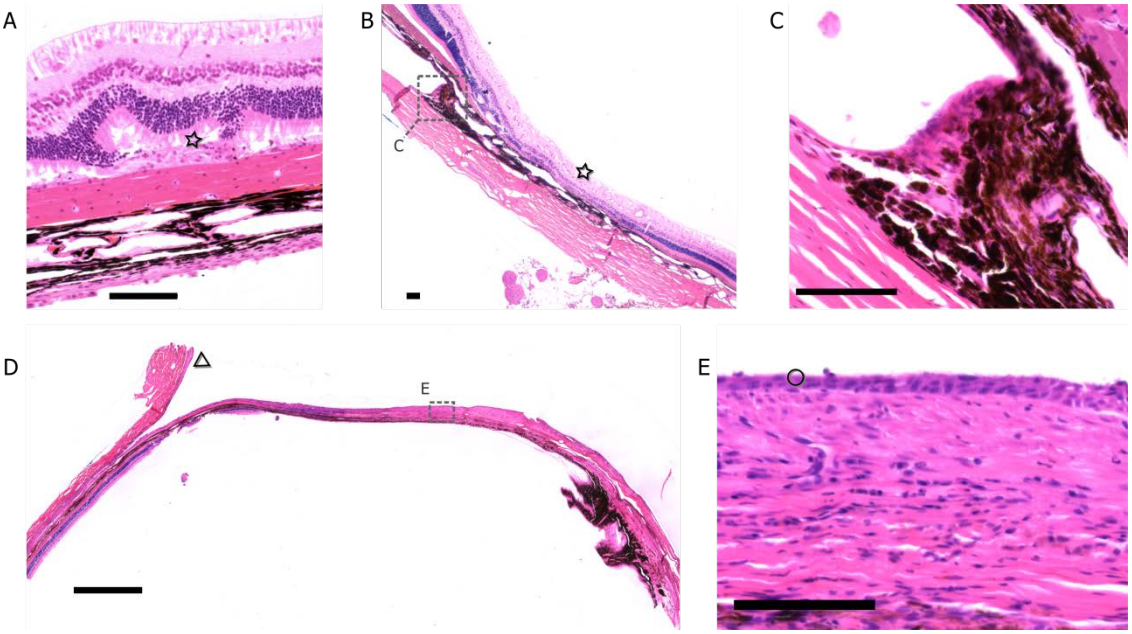

Fig. 9

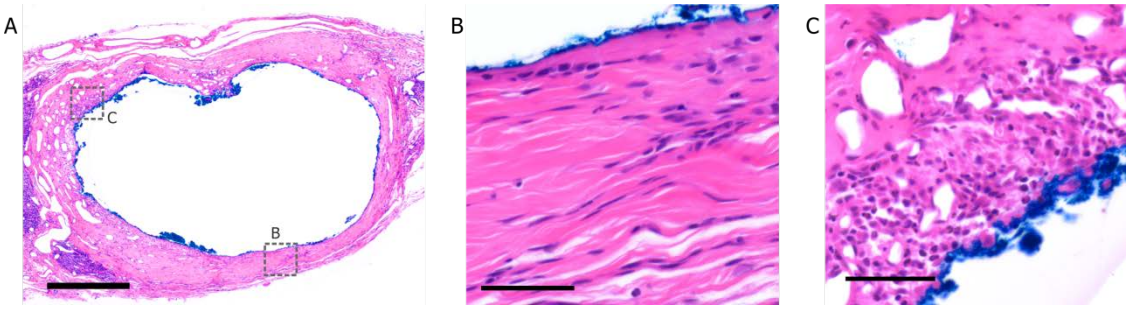

Fig. 10